CHEMISTRY OF MATERIALS

pubs.acs.org/cm

Article

Shape Control Beyond the Seeds in Gold Nanoparticles

Weilun Li,* Wenming Tong, Anchal Yadav, Eva Bladt, Sara Bals, Alison M. Funston,* and Joanne Etheridge*

Cite This: *Chem. Mater.* 2021, 33, 9152–9164

Read Online

ACCESS | Metrics & More | Article Recommendations | Supporting Information

ABSTRACT: In typical seed-mediated syntheses of metal nanocrystals, the shape of the nanocrystal is determined largely by the seed nucleation environment and subsequent growth environment (where "environment" refers to the chemical environment, including the surfactant and additives). In this approach, crystallinity is typically determined by the seeds, and surfaces are controlled by the environment(s). However, surface energies, and crystallinity, are both influenced by the choice of environment(s). This limits the permutations of crystallinity and surface facets that can be mixed and matched to generate new nanocrystal morphologies. Here, we control post-seed growth to deliberately incorporate twin planes during the growth stage to deliver new final morphologies, including twinned cubes and bipyramids from single-crystal seeds. The nature and number of twin planes, together with surfactant control of facet growth, define the final nanoparticle morphology. Moreover, by breaking symmetry, the twin planes introduce new facet orientations. This additional mechanism opens new routes for the synthesis of different morphologies and facet orientations.

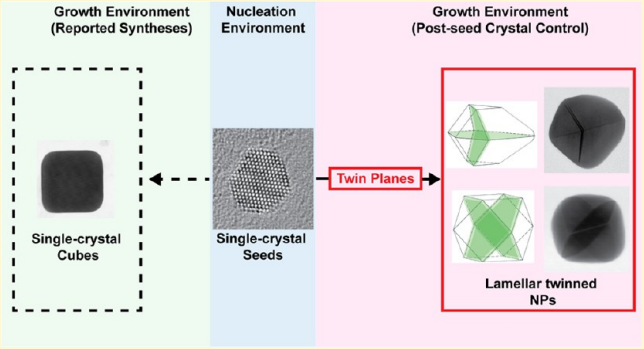

INTRODUCTION

Understanding and controlling the shape and morphologies of metal nanoparticles is fundamental to their development for applications in many fields, including optoelectronic,[1−3] sensing,[4,5] catalysis,[6−8] and biomedical sciences.[9−11] However, despite intense research over several decades, the growth of nanoparticles remains a largely empirical activity, with full details regarding the underlying mechanisms still unclear.

The seed-mediated approach aims to separate the synthesis of nanoparticles into two steps, each with a chosen chemical environment: the rapid formation of monodisperse seeds (seed nucleation environment) and the subsequent controlled growth of the seeds into the desired shape (growth environment).[12] The control over nanoparticle crystallinity is normally achieved during the formation of seeds because at tiny sizes there is a relatively low energy cost for structural change. In subsequent growth, the crystallinity is not modified from that of the seed.[13−15] In this way, the crystallinity of the final nanoparticle is expected to be consistent with the seeds. Based on this, single-crystal seeds can lead to single-crystal nanoparticles with shapes ranging from spheres, rods, cubes to octahedra, with control over these given by the effect of facet-directing surfactants and/or additives. In contrast, seeds that incorporate twin planes are known to result in the growth of right bipyramids, nanoplates or decahedrons, and icosahedrons depending on the number and orientation of twin planes.[16−19] However, as the nucleation environment used to synthesize seeds is also surface active,[20] the resultant seeds have facets and defects characteristic of this environment, limiting morphologies achievable in the subsequent growth phase.

Within seed-mediated syntheses, the seed nucleation environment is designed to achieve good monodispersity and control the crystallinity of the seeds (and hence the final nanoparticle). In contrast, the growth environment is tuned to achieve controlled growth of specific surface facets. However, the control over crystallinity and surface facets is not fully independent but limited by synthetic conditions, such as the surfactant and growth rate. For example, to synthesize gold nanocubes bound by {100} facets, surfactants such as cetyltrimethylammonium bromide (CTAB) are added to the nucleation and growth environments to facilitate the preservation of {100} facets relative to the {111} facets.[12] (For metallic bulk gold, the energy of surface facets, in the absence of surfactants, follows the sequence {111} < {100} < {110}.[21]) However, the use of such surfactants also affects the crystallinity of the seeds. For example, seeds grown in CTAB are single crystal, while seeds grown in citrate are predominantly multiply twinned.[20] In addition to surfactants, growth rate can be a mechanism for controlling crystallinity.

Received: July 16, 2021
Revised: November 15, 2021
Published: November 30, 2021

https://doi.org/10.1021/acs.chemmater.1c02459
Chem. Mater. 2021, 33, 9152–9164

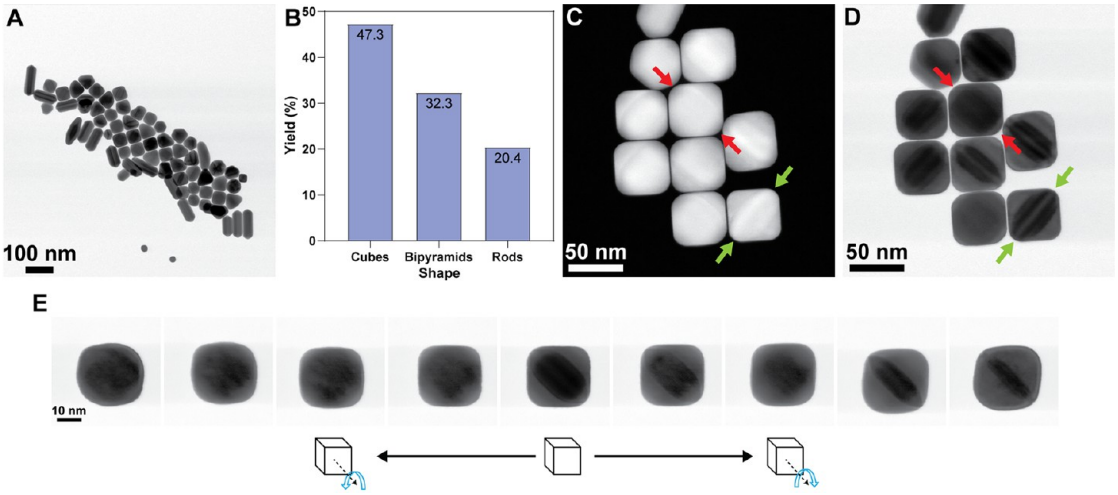

Figure 1. Final growth products using "post-seed crystal control," after growing seeds in the growth solution for 48 h. (A) Overview BF-STEM image. (B) Summary of shape yield of the final growth products following an analysis of 260 particles. Higher-magnification HAADF-STEM (C) and BF-STEM (D) images of gold nanocubes showing "striped" contrast across the diagonal. (E) BF-STEM images of the tilt series of a representative cube around the ⟨100⟩ zone axis for ±20°.

Here, we explore this possibility using gold nanocubes as a model system.

Among the many different shapes that can be generated in metal nanoparticle syntheses, a gold nanocube is perhaps the simplest, a natural consequence of the cubic unit cell of gold. Gold nanocubes are generally thought to be single crystals, bound by six {100} surface facets.[22] This simple structure has encouraged the use of gold nanocubes as a fundamental system to study nanoparticle growth mechanisms, such as facet growth[23,24] and symmetry breaking.[25,26] They have also been used in applications, such as plasma coupling[27,28] and self-assembly.[29] The basis of these studies is that the crystallinity and morphology of gold nanocubes are well understood, namely a single-crystal cube. In a typical seed-mediated synthesis of gold nanocubes, it is plausible that the nanocubes would be single crystals because: (1) the seeds grown in CTAB are single-crystal cuboctahedra.[20,30] To form a cube, the shape evolution only requires the deposition of gold on the {111} facets to be faster than that on the {100} facets. During this growth, the crystallinity of nanoparticles remains unchanged as single crystals; (2) the shape of nanocubes is the same as the unit cell it is built from, the cubic unit cell of gold. The presence of defects would break this symmetry. For example, twin planes might be expected to lead to mirrored growth of the nanoparticle, resulting in a right bipyramid, bisected by the twin plane in the middle of particles, as has been observed previously.[31]

"Twinning" is a common phenomenon in the growth of gold nanoparticles due to the low stacking fault energy of gold. In the face-centered cubic (fcc) structure of gold, a perfect crystal has close-packed {111} planes stacked with the sequence "ABCABCABC." When this stacking is disrupted by a missing or additional atomic plane, e.g., "ABCABACBA," a twin plane B is formed with the structure mirrored on each side of the plane.

Twin planes can play an important role in shape and facet control and hence in the functionality of nanoparticle systems. A number of experimental observations have shown that twin planes can lead to a mirroring of the external particle shape, analogous to the mirror of internal atomic planes.[31] In this way, twin planes can influence the final shape of the nanoparticle by defining the shape symmetry, for example, single-twinned bipyramids and penta-twinned decahedrons.[31−33] Twin planes are also reported to affect the growth habit and surface activity of nanoparticle facets. For example, it has been suggested that twinning in silver nanocubes is responsible for their nonunity aspect ratio (length/width not equal to one),[34] and that planar defects in nanoplates are key to their highly anisotropic shape.[33] Similarly, a study of twinned silver nanocubes observed selective etching of the {111} facets parallel to the twin plane, suggesting the modification of surface activity by twin planes.[35] Recently, the selective metal oxidation driven by planar defects has been revealed by in situ high-resolution transmission electron microscopy.[36]

In addition to the important role in controlling the nanoparticle morphology, twin planes are often found to greatly enhance catalytic activity. For example, single-twinned palladium right bipyramids show 2.5 times increased activity in formic acid oxidation compared with single-crystal palladium cubes.[37] Similarly, platinum icosahedral nanocrystals with twin planes show 4 times increased activity in an oxygen reduction reaction when compared with their single-crystal counterparts enclosed by the same {111} facets.[38] Observations such as these have encouraged the development of methods to deliberately incorporate planar defects into nanoparticles, for example, using plasmon mediation[34] and ultrafast lasers.[39]

Here, we combine single-crystal gold seeds with twin insertion during post-seed growth in the presence of CTAB, to synthesize different gold nanoparticle morphologies, including twinned nanocubes and right bipyramids. The type (parallel or cyclic) and number of twin planes incorporated during the growth, together with environment control of surface chemistry, determines the final shape of nanoparticles. Using aberration-corrected transmission electron microscopy (TEM), we characterize the three-dimensional morphology and atomic-scale structure of nanoparticles with incorporated twin planes. Finally, the products of the reported nominally "single-crystal" gold nanocube synthesis is reviewed, and notably, we find the presence of twinned nanocubes within the products, not reported previously.

https://doi.org/10.1021/acs.chemmater.1c02459
Chem. Mater. 2021, 33, 9152−9164

RESULTS

Postseed Crystal Control. The synthetic approach developed here combines the seed-mediated approach with rapid subsequent growth of seed particles in the growth environment to deliberately incorporate defects, in the form of twin planes, into nascent post-seed particles, changing their crystallinity relative to that of the seeds. It exploits the idea that the final nanocrystal morphology can be controlled by employing different surface energies and/or different defect incorporation at the seed and/or growth steps, increasing available elements that can be mixed and matched to control shape.[21]

To highlight the potential utility of this approach, single-crystal seed nanoparticles are used. These are synthesized via the rapid reduction of the gold(III) precursor to gold(0) with borohydride, in the presence of the surfactant CTAB. The resultant seeds are predominantly single-crystal cuboctahedra around 2 nm in diameter.[20,30] Rapid growth of seed particles upon injection into the growth solution is achieved using a high mole ratio of the reductant, ascorbic acid, combined with a relatively high concentration of seeds (relative to synthetic conditions used to synthesize single-crystal cubes[12,40]). CTAB was selected as the surfactant to preserve the {100} facets. Given the low formation energy for twin planes in gold, this rapid growth leads to the incorporation of a high number of twin planes in nanoparticles, which are absent in seed particles. Growth via coalescence also leads to the incorporation of twin planes. The final nanocrystalline products incorporate predominantly either one, two, or three (lamellar) twin planes. Products incorporating two (lamellar) twin planes take on a cubic morphology, while those with one or three (lamellar) twin plane defects form right bipyramids.

An overview of the colloid formed from this synthesis is presented in Figure 1. As highlighted in Figure 1A,B, nanoparticle morphologies obtained from the synthesis include cubes (47%), right bipyramids (32%), and rods (20%). We note that no shape purification was carried out on this relatively shape polydisperse sample, as the aim is to demonstrate proof of concept. The edge length of cubes and right bipyramids are similar (48 ± 2 and 50 ± 4 nm, respectively, for the length of the {100} facets), while the diameter of rods is 38 ± 2 nm.

Care was required for the deduction of the 3D shape from 2D projections in the image. The cubes tend to lie with a {100} face parallel to the support film on TEM grids, and therefore perpendicular to the electron beam, appearing in projection as squares in scanning transmission electron microscopy (STEM) images. However, particles with other shapes are more likely to have several possible stable orientations on the support film and hence relative to the electron beam. For example, by comparing with thickness profiles of particle models (measured from a quantitative analysis of high-angle annular dark-field (HAADF) STEM images[41]), particles with triangular shapes in the 2D image were determined to be projections of right bipyramids.

Figure 1C,D shows magnified images of cubes using high-angle annular dark-field scanning transmission electron microscopy (HAADF-STEM) and bright-field (BF) STEM. If a gold nanocube is a single crystal, it should generate a uniform intensity distribution in a ⟨100⟩ zone-axis TEM image. However, close examination of cubes reveals stripes along their diagonals (e.g., the cube indicated by green arrows in Figure 1C,D). We note that the striped contrast is not always obvious in these cubes (e.g., the cube indicated by red arrows in Figure 1C,D). To examine this, a series of BF-STEM images were taken of a representative cube tilted around the ⟨100⟩ zone axis for ±20°. The contrast changes with the view direction, and stripes are only visible in one tilt direction away from the ⟨100⟩ zone axis (Figure 1E). By examining more than 50 individual cubes, that is, by tilting each cube to several different view directions, all of the cubes were determined to contain these stripe features (we cannot exclude the possibility that there may be an extremely small percentage that do not show stripe features, but we did not observe any). This indicates that gold nanocubes synthesized with this post-seed crystal control method are not single-crystal cubes.

To determine the crystalline structure of these nanocubes, we analyzed the corresponding selected area diffraction patterns (SADP). In the ⟨110⟩ zone-axis pattern, in addition to the main reflections (circled in red), there are also short lines located at positions that mirror that of the main reflections (in green) (Figure 2D). The mirrored position of

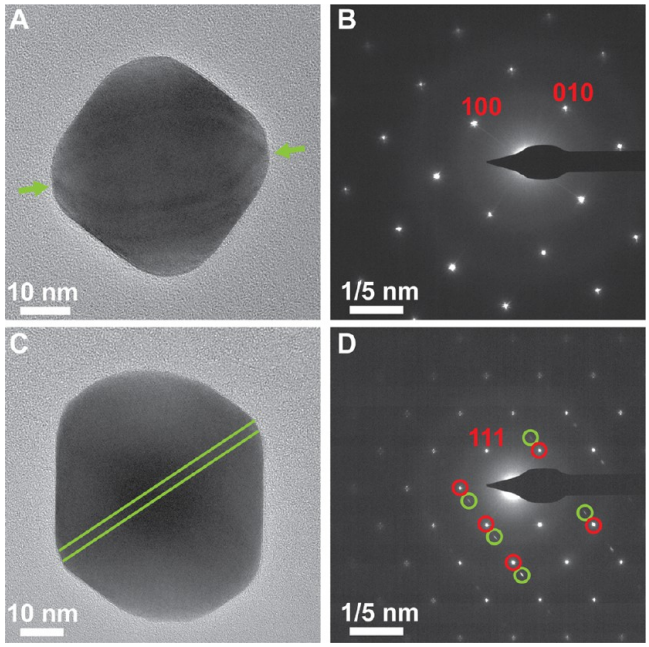

Figure 2. Phase-contrast TEM images and corresponding SAD patterns from twinned gold nanocubes oriented along the (A,B) ⟨100⟩ zone axis and (C,D) ⟨110⟩ zone axis. (B) and (D) are SAD patterns taken from the nanocubes in (A) and (C), respectively. The green arrows in (A) indicate twin planes in the cube, and the green lines in (C) indicate twin planes parallel to the electron beam.

diffraction spots is consistent with the presence of a twin domain, as is the elongation of these spots ("shape transforms") in the ⟨111⟩ direction, which is normal to the twin plane in the corresponding image, highlighted by green lines in Figure 2C. The ⟨100⟩ zone-axis TEM image clearly shows the contrast of twin planes inside the cube (indicated by green arrows); however, the SADP shows a typical square pattern of diffraction spots, as if it is taken from a single-crystal gold nanoparticle (Figure 2A,B). This is because reflections from different twin domains overlap in this orientation, giving the illusion of a single crystal.

Characterization of Twinning Defects. To gain a better understanding of the shape and internal structure of these gold

https://doi.org/10.1021/acs.chemmater.1c02459
Chem. Mater. 2021, 33, 9152−9164

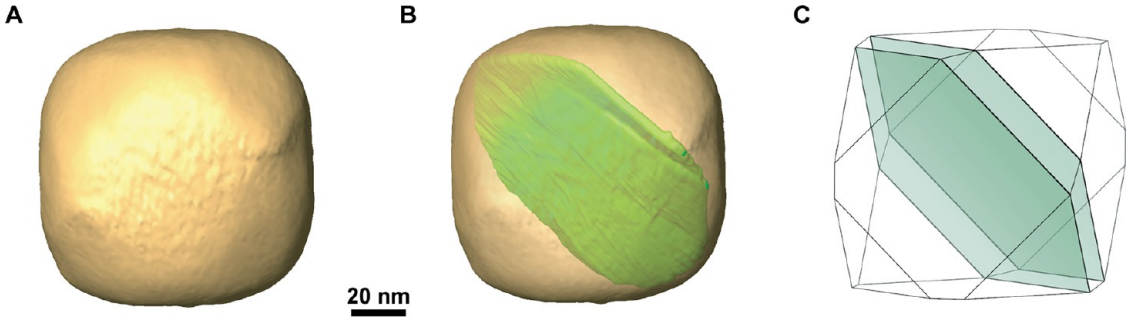

Figure 3. Representative twinned gold nanocube reconstructed by multimode electron tomography. (A) Solid model shows the cubic shape and {111} facets at corners and (B) the transparent model indicates the twin lamella (in green) inside the twinned cube. (C) Reconstructed particle model.

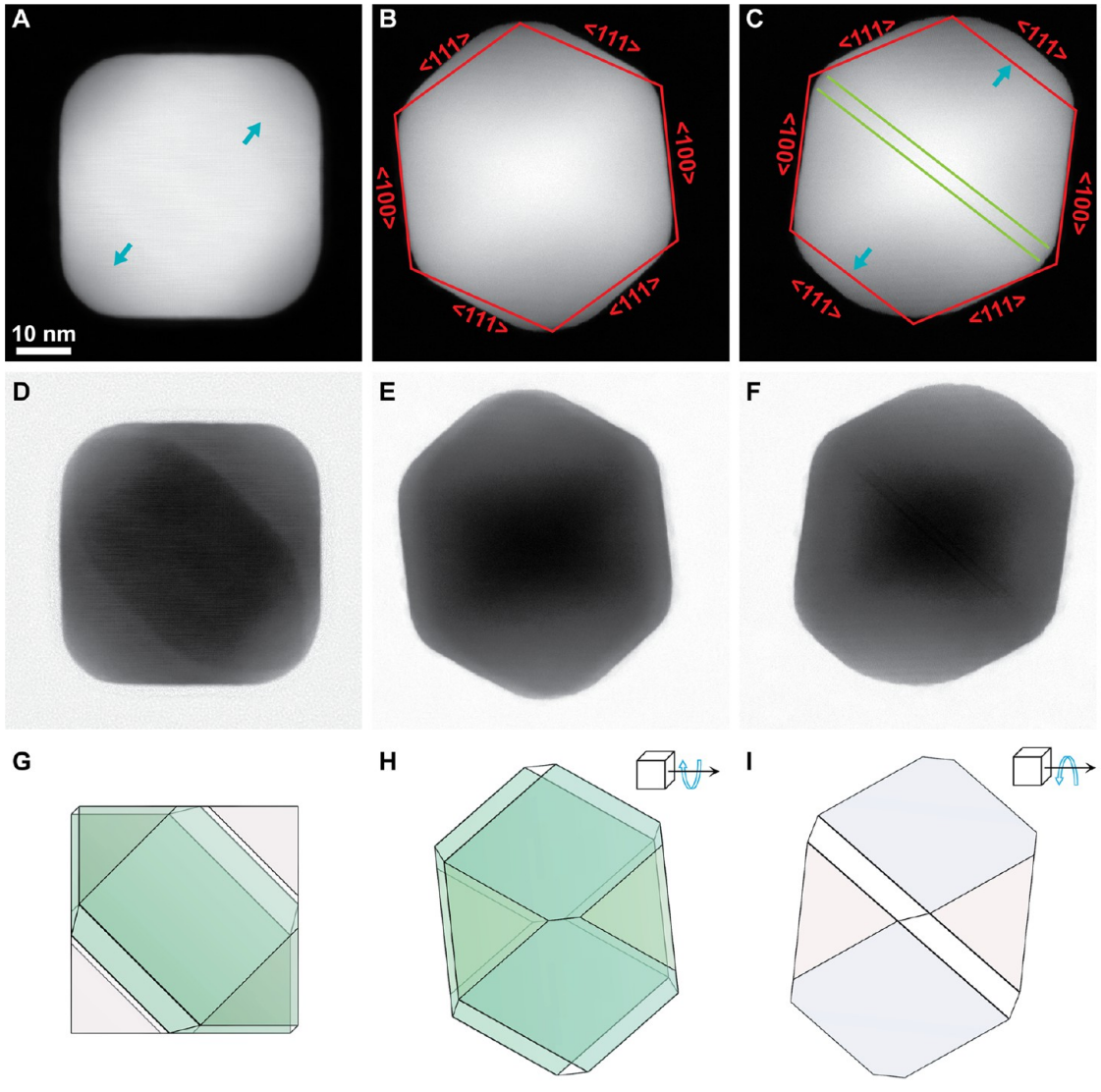

Figure 4. Representative gold nanocubes viewed along the: (A,D,G) ⟨100⟩, (B,E,H) ⟨110⟩, and (C,F,I) ⟨1$\bar{1}$0⟩ zone axes. In each view direction, HAADF-STEM (A−C) and BF-STEM (D−F) images were taken and compared with the cube model below (G−I). In the cube model, all of the corners are truncated by {111} facets and two (111) twin boundaries spanning the diagonal are shown in green ({100} facets in light blue and {111} facets in pink). Two of the corners that are parallel to twin planes (indicated by arrows in (A,C)) have smaller truncating {111} facets than the other two corners, resulting in an anisotropic shape of this twinned cube.

cubes, a multimode electron tomography experiment was carried out to characterize the location of twin planes and the shape of the cube in three dimensions simultaneously.[42] During the acquisition, a tilt series of projection images were acquired using two different ADF detectors with different collection ranges. The HAADF-STEM reconstruction is used

https://doi.org/10.1021/acs.chemmater.1c02459
Chem. Mater. 2021, 33, 9152−9164

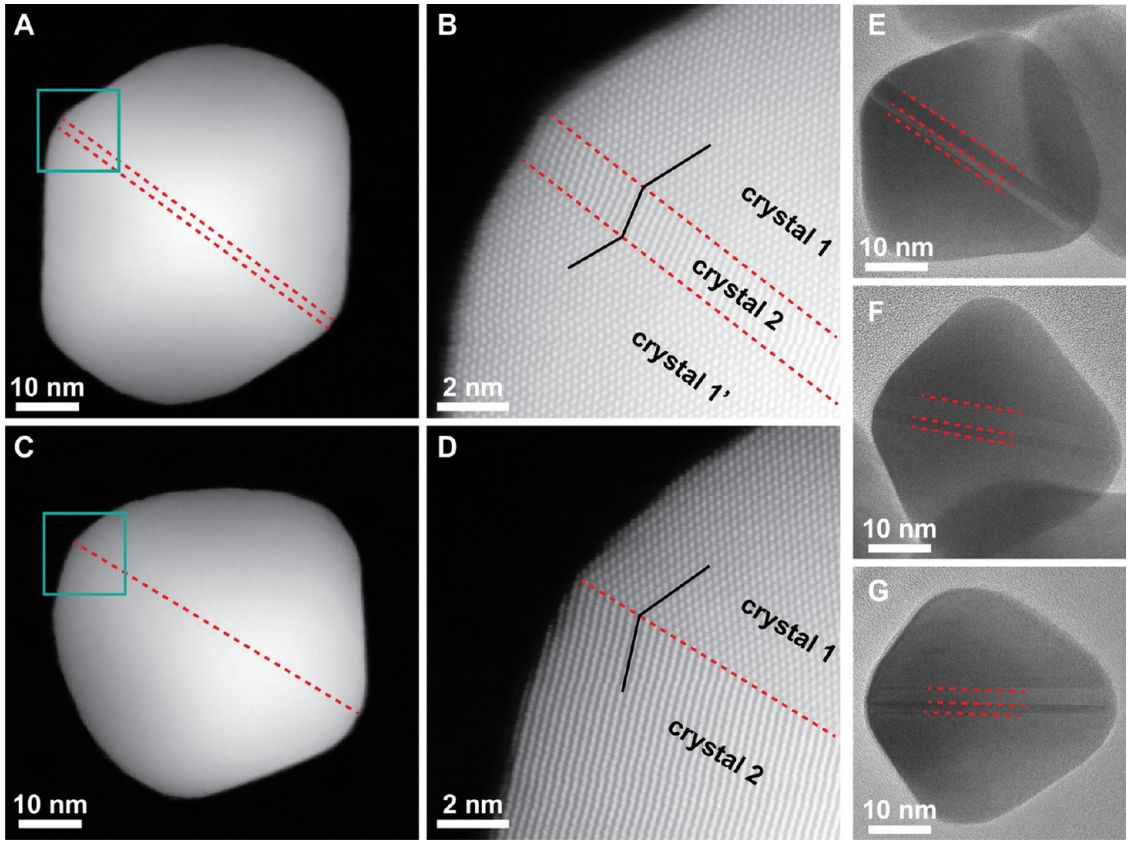

Figure 5. Representative ⟨110⟩ zone axis HAADF-STEM images of (A,B) a twinned cube (with corners truncated) with two parallel twin boundaries and (C,D) a right bipyramid with one twin boundary. Panels (B,D) are enlarged images of the regions marked by orange boxes in (A,C). (E−G) ⟨110⟩ zone-axis TEM images of right bipyramids with three parallel twin boundaries. Enclosed by {100} facets, an odd number of parallel twin boundaries results in a right bipyramid, while an even number of parallel twin boundaries results in a cube.

to retrieve the morphology of the nanocube, and the low-angle annular dark-field (LAADF) STEM tilt series generates contrast arising from an interior twin lamella, allowing its 3D reconstruction (Figure S1). The cubic shape of the particle and {111} truncations at its corners are evident in Figure 3A. The twin crystal with an orientation different from the cube is shown in green in Figure 3B. A corresponding particle model is reconstructed in Figure 3C. A movie of the tomogram by LAADF-STEM images is available in Movie S1.

Figure 4 shows HAADF-STEM and BF-STEM images of cubes along three different major zone axes: ⟨100⟩, ⟨110⟩, and ⟨1$\bar{1}$0⟩. These are able to be compared with a hypothetical cube model with truncated corners (Figure 4G−I). Two {111} planes have been drawn in green at the center of the model cube. HAADF-STEM images are sensitive to the particle thickness, so outline the projected shape of the cubes, whereas BF-STEM images are sensitive to the internal structure inside the cubes. Consider first the cube oriented in the ⟨100⟩ zone axis (Figure 4A,D,G). The cube is bound by {100} facets. The HAADF-STEM image has lower intensity at the corners of the cube, indicating that the "cube" is thinner at the corners, which are truncated by {111} facets. Moreover, two corners highlighted by arrows generate higher image intensity than the other two corners, indicating that the cube corners are not truncated equivalently. In the corresponding BF-STEM image, the dark oval shape in the middle of the projected cube is consistent with the projection of {111} planes highlighted in light green color in the cube model. One possible structure consistent with the contrast observed here is a lamellar twin crystal with an even number of twin boundaries in parallel.[33,43,44]

In the ⟨110⟩ zone axis, except for two {001} facets, the observation of {111} facets confirms that the cube corners are truncated. The twin planes are now perpendicular to the electron beam and appear as a hexagonal projection in the BF-STEM image (Figure 4E). In the ⟨1$\bar{1}$0⟩ zone axis, the twin planes are parallel to the electron beam so that they do not generate contrast in this projection. The experimental observations agree well with the reconstructed particle model of a cube with {111} truncation facets at eight corners and {111} twin planes close to the cube diagonal. However, for the two corners indicated by arrows in Figure 4C, {111} facets parallel to the twin planes are markedly less truncated than other {111} facets, consistent with the observation in the HAADF-STEM image in Figure 4A.

As noted earlier, direct evidence for the presence of twin planes was obtained by taking selected area diffraction patterns (SADP) (Figure 2D). Together with observations in the tomograms of Figure 3 and zone-axis images in Figure 4, the shape of the twin plane is determined to be hexagonal, and it is located close to the cube diagonal.

We observe that particle shapes arising from this synthesis depend on the number of twin boundaries. The cube-shaped particles comprise two (or an even number) of (111) twin boundaries closely spaced near the center of the cube (see the ⟨110⟩ zone-axis image in Figure 5A,B). These boundaries separate the particle into three domains. Crystal 1 and crystal 1′ have the same orientation and delineate the cubic shape.

https://doi.org/10.1021/acs.chemmater.1c02459
Chem. Mater. 2021, 33, 9152−9164

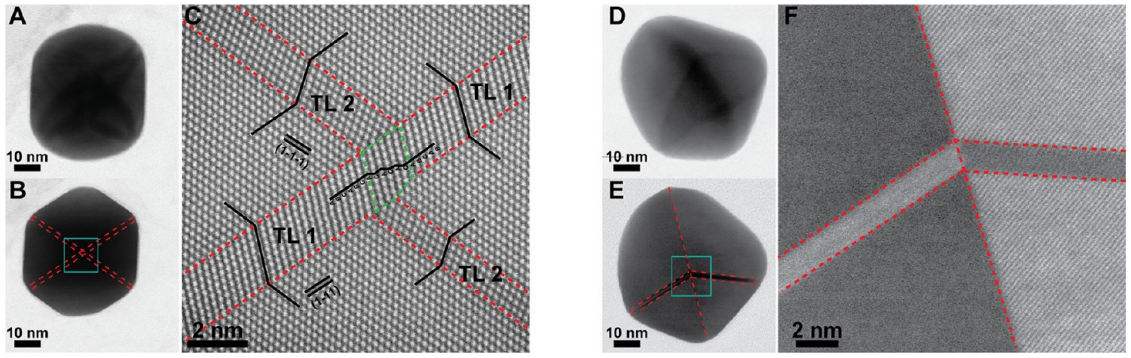

Figure 6. (A–C) Representative cube with lamellar twins intersecting at the center of the particle. (A) BF-STEM image of a cube oriented to show the projections of both twin boundaries. (B) ⟨110⟩ zone-axis HAADF-STEM image of the cube with the two intersecting twin boundaries parallel to the electron beam. (C) Atomic-resolution HAADF-STEM image of the intersecting twin lamellae marked by the orange box in (B). (D–F) Representative right bipyramid with two intersecting twin lamellae. (D) BF-STEM image of the right bipyramid in an orientation that reveals the two intersecting twin lamellae. (E) ⟨110⟩ zone-axis BF-STEM image of the right bipyramid with the twin boundaries parallel to the electron beam. (F) BF-STEM image of the region marked by the orange box in (E) showing the twinning structure of the right bipyramid. Red dashed lines in (C, F) indicate twin boundaries. Green dashed lines in (C) indicate the hcp phase at the junction of twin lamellae in the twinned cube.

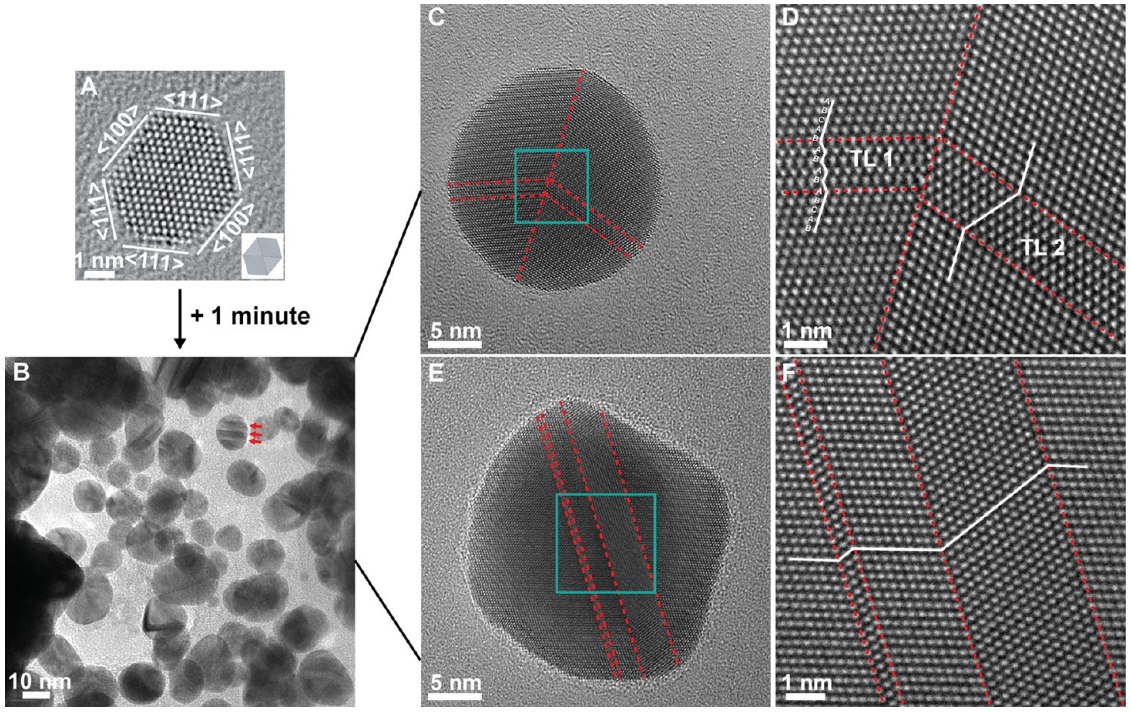

Figure 7. Phase-contrast TEM images of (A) a representative seed particle, a single-crystal cuboctahedron in the ⟨110⟩ zone axis, and (B–F) particles grown from the seeds in the growth solution for 1 min. Particles in (B–F) are viewed along the ⟨110⟩ zone axis. Arrows in (B) indicate parallel twin boundaries. Dashed red lines in (C–F) indicate twin planes. Panels (D,F) are the enlarged images of the regions marked by black boxes in (C, E).

Crystal 2 between the two twin boundaries is the twin lamella with a mirrored crystallographic orientation relative to the rest of the cube.

In contrast, nanoparticles with an odd number (either 1 or 3) twin planes have a right-bipyramid geometry. These are also bound by {100} facets; however, the entire particle is bisected into two domains (crystal 1 and crystal 2) whose structure is mirrored with respect to each other, generating a right bipyramid (Figure 5C–G). The orientation of the domain is mirrored after crossing each of the three twin boundaries, analogous to the single-twinned right bipyramids (Figure 5C,D). In the case of three twin boundaries (Figure 5E–G), contrast changes evidently across twin boundaries indicate the change in crystallographic orientation across twin planes.

A correlation between the number of twin boundaries and the shape of gold nanoparticles is evident. Cubes and right bipyramids are both bound by {100} surface facets (aside from their {111}-truncated corners). The difference in shape originates from the number of parallel twin boundaries: right bipyramids contain one (or three) twin planes, while twinned cubes contain two twin planes. This arises naturally from the fact that two twin boundaries in parallel can effectively cancel the impact of each on the symmetry of the external shape. This observation agrees with models of lamellar twinned particles

https://doi.org/10.1021/acs.chemmater.1c02459
Chem. Mater. 2021, 33, 9152–9164

proposed in the lateral growth of silver and copper nanoplates.[33,45−47]

Interestingly, some cubes are observed to contain intersecting twin lamellae, such as are evident in the BF-STEM image of Figure 6A. The dark contrast across the diagonals indicates the two twin lamellae, which intersect in the middle. In the ⟨110⟩ zone-axis image, two intersecting twin boundaries are parallel to the electron beam (Figure 6B). In this orientation, it can also be seen that the projected shape is divided by two intersecting lamellae into four domains. It is evident that having twin lamella on opposite cube diagonals "corrects" the break in symmetry (of {111} truncation facets) that is introduced by a twin lamella on only one diagonal (for example, the twinned cube in Figures 4C and 5A).

The atomic structure at the twin intersection is revealed in Figure 6C. Since the twin lamella 1 (TL1) is parallel to the $(1\bar{1}1)$ plane and the TL2 is parallel to the $(\bar{1}\bar{1}1)$ plane, defects are generated at the junction. The stacking sequence in TL1 near the twin junction changes from fcc to hcp; "ABCABCACACACABCAB" (outlined by green dashed lines). The lattice arrangement in TL2 is totally disrupted, displaced, and reduced in thickness, by the penetration of TL1.

Twin lamellae are also apparent in right bipyramids (Figure 6D−F). A high-resolution BF-STEM image reveals the orientations of different domains (Figure 6F). A single twin boundary bisects the particle, with two twin lamellae mirrored across it, with the intersection just off the center of the particle. We note that the detailed atomic structure cannot be fully resolved due to the instability ("rocking") of the right bipyramid on the support film in this orientation.

The remaining 20% of the final products of this synthesis are nanorods. The contrast in BF-STEM images suggests that these also contain twin boundaries (Figure S2) and is consistent with the penta-twinned structure of gold nanorods grown in the absence of silver ions.[48,49]

Characterization of Seeds. The crystallinity and morphology of seed particles used here were characterized by atomic-resolution TEM. The electron dose was kept very low to ensure that the pristine structure was examined and any twin planes we observed were not a consequence of beam damage, as it is well known that high-energy electrons can induce structural changes in small gold nanoparticles.[30] The seeds were observed to be predominantly single crystal (57 out of 78 seed particles, 73%) (Figure 7A), although a small percentage of twinned seed particles were also observed (Figure S3). This is consistent with our previous detailed low dose, aberration-corrected TEM study of gold seeds synthesized using the same protocol which were observed to be predominantly single-crystal cuboctahedra bound by alternating {100} and {111} surface facets.[30] This observation is also consistent with early atomic-resolution TEM characterization of the structure of gold seeds synthesized in CTAB,[20] where single-crystal seeds account for at least 72% of the seeds (106 out of 147 seeds).

Characterization of Particles at Early Stages of Growth. Almost all of the final products examined in this synthesis contain twin boundaries. The finding that the final products show that the incorporation of twin boundaries is a new observation, as it is well accepted that the final crystallinity of nanoparticles grown via the seed-mediated method reflects that of the seeds.[17,21] To investigate the mechanism by which twinned structures form, particles at the early stages of growth were characterized.

Growth of the seeds for 1 min (in the growth solution) results in an increase in the average particle size from 4 to 20 nm, indicating a rapid initial growth rate. The seed evolves from a cuboctahedron bound by {100} and {111} facets (Figure 7A) to a particle morphology that is either pseudospherical with undefined facets or irregular (Figures 7B and S4). TEM images suggest two modes of growth: (1) overgrowth by atom deposition (Figures S4 and S5) and (2) coalescence (Figures S4 and S6). In both cases, a large number and variety of twinning defects are incorporated into the growing particles. We note that nucleation of additional seed particles is very unlikely given the reductant, ascorbic acid, has insufficient reducing strength under these conditions to fully reduce gold(III) to gold(0). No evidence of particles comparable to the size expected for seeds was evident at 1 min (Figure S7).

As one typical example, the particle in Figure 7C,D has a twinning structure reminiscent of the structure in the right bipyramid in Figure 6D−F. Interestingly, the region denoted TL2 in Figure 7D has the commonly observed lamellar twin structure with two parallel twin boundaries, whereas TL1 has an hcp structure. The hcp structure is generally rarely observed in gold nanoparticles as it is a higher energy structure, at least in the bulk. Here, it is observed for many of the small right bipyramids with twin lamellae after 1 min of growth. A recent study has suggested that the seed-mediated synthesis of gold nanostars occurs via the hcp phase by kinetic control with a rapid growth rate facilitating the formation of the energetically unfavorable hcp phase.[50,51] The hcp structure observed here within the complex twinning structures of right bipyramids and cubes might result from the need to accommodate the misorientation between the twin lamellae.

Figure 7E,F shows a second particle morphology frequently observed after 1 min of growth. The particle shows a series of parallel twin planes, each spanning a variable number of atomic rows. The final products of the synthesis contain predominantly one or two (or at most three) parallel lamellar twin plans. The particle shown in Figure 7E has an even number of twin planes, lying parallel to one another, along with a roughly cubic-looking morphology. The final cube products also have an even number (two) of lamellar twin planes. Although the surface facets of the particle cannot be determined at this early stage of growth, we propose that particles with an even number of parallel twin boundaries evolve into a twinned cube during subsequent growth, while particles with an odd number of twin planes form right bipyramids. In both cases, where there is a larger number of twin planes in the early stages of growth, a reduction of twin planes with time is required, for example, via coalescence of pairs of twin planes. This type of "detwinning process" has been proposed to be energetically favorable during nanoparticle growth.[43]

In addition to these pseudospherical particles, irregularly shaped particles tend to be much larger, have no consistent shape, and exhibit multiple twin planes located in apparently arbitrary locations within the particles (Figures S4C and S6). The process of coalescence involved in the formation of these particles is also thought to result from the fast growth rate, rather than the destabilization of the CTAB bilayer. The solutions are maintained above the critical micelle concentration (cmc) of CTAB at all times during the synthesis of twinned nanocubes; therefore, particles maintain a CTAB bilayer. It is also apparent that the CTAB is preserved on the

https://doi.org/10.1021/acs.chemmater.1c02459
Chem. Mater. 2021, 33, 9152−9164

surface of 1 min growth products and 48 h final products as observed by TEM (Figure S8).

Remarkably, this large variety of pseudospherical and irregular particle shapes, sizes, and twin configurations ultimately resolve into a colloid with just three major products, each with its own highly specific twin configurations and low size and shape polydispersity.

Reported Synthesis of Gold Nanocubes. In this section, we revisit the morphology and crystallinity of nanocubes formed via the reported seed-mediated synthesis. Figure 8 shows the BF-STEM images of nanoparticles synthesized using the reported synthetic conditions[12,40] for single-crystal gold nanocubes. Inspection of the images shows stripes along their diagonal in the BF-STEM image (Figure 8B), similar to the contrast observed in the cubes containing twin planes in Figure 1D. By similarly examining more than 50 individual cubes (by tilting each cube to different view directions), ~20% of the cubes were determined to contain similar stripe features. This indicates that cubes synthesized with this method are, in fact, a mix of cubes possessing different structures: single-crystal cubes and non-single-crystal cubes. Further analysis using SADP shows that the non-single-crystal cubes are in fact twinned. Upon reviewing the literature, we find that this is common to the reported synthesis of gold, copper, silver, and core−shell nanocubes; this will be discussed later.

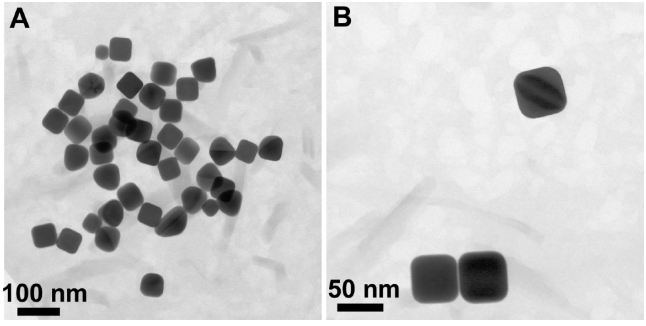

Figure 8. Reported synthesis of gold nanocubes: BF-STEM images of the reported seed-mediated synthesis of gold nanocubes aimed at the production of single-crystal gold nanocubes. (A) Overview image showing a mix of single-crystal cubes and twinned cubes. (B) Higher-magnification image highlighting the contrast across the cube diagonal due to twin boundaries.

DISCUSSION

Postseed Crystal Control Method. Based on the observations above, we propose a mechanism for the growth of twinned nanocubes in Figure 9. It involves three stages: (1) gold atoms nucleate and evolve into seeds with a relatively stable single-crystal cuboctahedral structure in the nucleation environment; (2) seeds, once added into the growth environment, grow very rapidly in size (via atom deposition and/or coalescence) with the accompanying incorporation of twinning defects; (3) particles with their various twin structures further evolve into three major final products, each with its own distinct twin structure.

All of the final growth products—cubes, right bipyramids, and rods—are dominated by {100} surface facets, despite having evolved into different shapes, showing effective preservation of {100} facets by the use of CTAB. It also indicates that the configuration of twin boundaries is the deciding factor in determining whether the final shape will be a cube, right bipyramid, or rod.

As shown in Figure 7, nanoparticles at early growth stages have similar pseudospherical shapes (or larger irregular shapes) but different twinning structures. This, combined with the above observation, suggests that it is the twin boundaries incorporated post-seed that determines the final shape of the particles. As noted above, there is also a process of detwinning, resulting in just one, two, or sometimes three lamellar twin planes in the final product. For those particles containing an even number of twin boundaries, the external shape is a cube, whereas an odd number of twin boundaries leads to a right

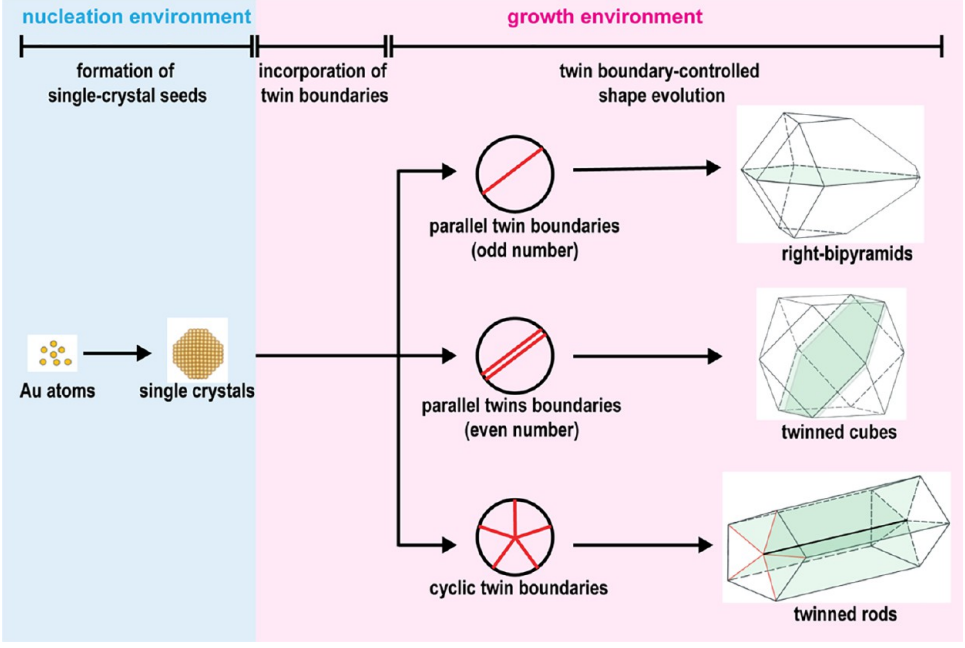

Figure 9. Schematic illustration of the growth pathway in rapid post-seed growth. The green planes and red lines indicate twin boundaries.

https://doi.org/10.1021/acs.chemmater.1c02459
Chem. Mater. 2021, 33, 9152−9164

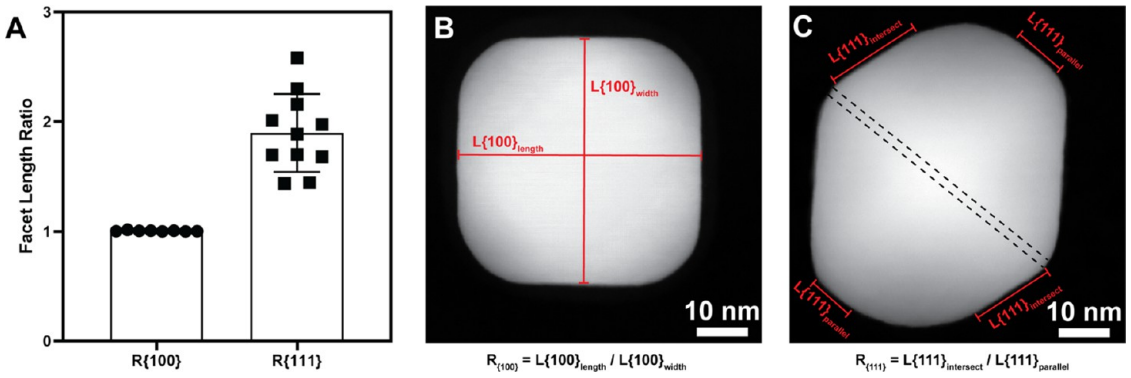

Figure 10. (A) Measurements of facet length of the post-seed synthesis final product. (B) Aspect ratio $R_{\{100\}}$ is determined by measuring the length and width of {100} facets from nanocubes in the ⟨100⟩ zone axis. $L\{100\}_{length}$ and $L\{100\}_{width}$ refer to the length of {100} facets along the longer side and shorter side, respectively. (C) Ratio $R_{\{111\}}$ is determined by measuring the length of {111} facets from nanocubes in the ⟨110⟩ zone axis. $L\{111\}_{intersect}$ and $L\{111\}_{parallel}$ refer to the length of {111} facets intersecting or parallel to twin planes, respectively. There are two $L\{111\}_{intersect}$ and $L\{111\}_{parallel}$ that can be measured, so the average distance is calculated.

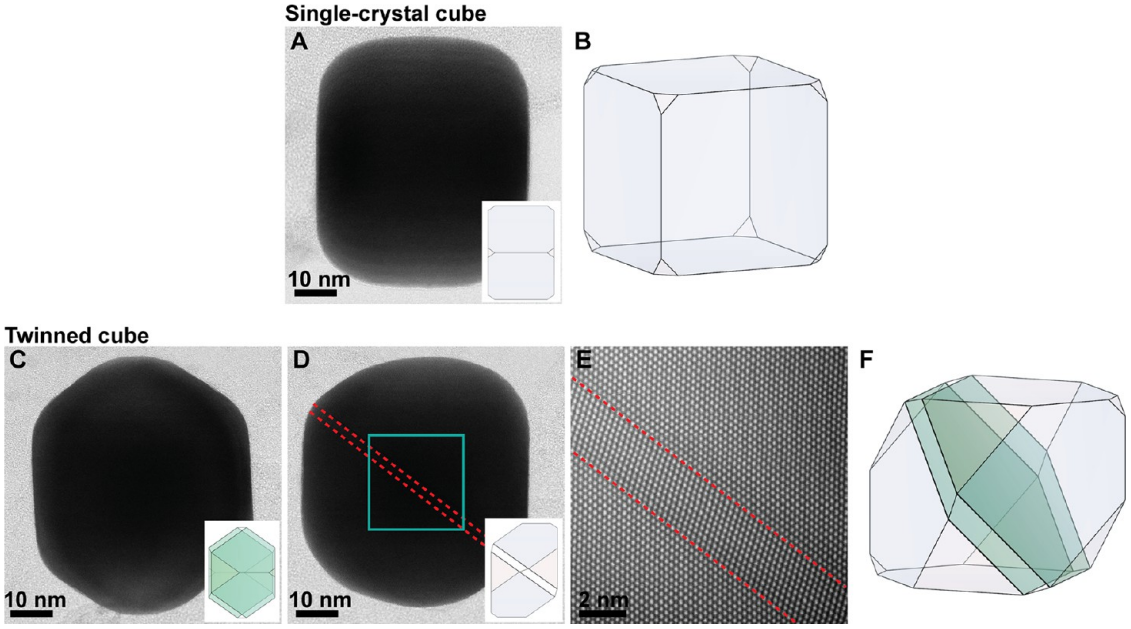

Figure 11. Reported synthesis of gold nanocubes: (A) single-crystal "cube" along the ⟨110⟩ zone axis and the reconstructed particle model (B). (C) Twinned cube oriented along the ⟨110⟩ zone axis with twin boundaries perpendicular to the electron beam. (D) Twinned cube orientated along the ⟨110⟩ zone axis with twin boundaries parallel to the electron beam. (E) Atomic-resolution HAAD-STEM image of the region marked by the box. (F) Particle model of the twinned cube. Green planes in particle models indicate twin planes. Red dashed lines in (D,E) indicate twin boundaries.

bipyramid. The penta-twinned particles tend to grow anisotropically along the longitudinal axis into penta-twinned rods, to minimize the total strain energy.[21,49]

There are a number of reports in literature that show transitions of crystallinity in gold.[13,52] Here, we have chosen a ligand system for which changes in crystallinity are well known and documented, to enable us to identify the incorporation of different types of twin planes.[53] Growth under these ligand conditions is known to lead to either single-crystal products or penta-twinned crystals. Yet, here, we see the incorporation of lamellar twin planes during growth.

In the case of twinned cubes, there are two necessary criteria for their preparation: the preservation of {100} surface facets and the inclusion of an even number of twin boundaries. Given the seeds prepared in the CTAB are predominantly single crystal, how are the lamellar twins introduced into the particles? The twinning structure in nanoparticles has been proven to be extremely sensitive to the growth kinetics.[34,54] In our study, the post-seed crystal control is demonstrated to be a facile, reproducible method of preparing twinned gold nanocubes in relatively high yield. After the formation of single-crystal seeds, we force the seeds to grow rapidly by increasing the concentration of the reducing agent (ascorbic acid in our case) in the growth solution. The rapid growth results in inclusion of parallel twin boundaries, which are crucial for the formation of a cubic shape. In this way, crystallinity and surface facets can be controlled separately by nucleation and growth environments, respectively. In the present proof-of-concept example, the combination of tuning the number of lamellar twin planes and {100}-type surfactant (CTAB) yielded twinned cubes or right bipyramids. This concept has the potential to be extended, for example, if seeds

https://doi.org/10.1021/acs.chemmater.1c02459
Chem. Mater. 2021, 33, 9152−9164

with different twin configurations are used, or single-crystal seeds are grown rapidly with a surfactant that preserves {111} facets (such as citrate[20]), additional new shapes may be possible.

It is noted that the yield of twinned cubes is higher than right bipyramids, indicating that the particles are more likely to have an even number of twin boundaries. It has also been observed elsewhere that in the synthesis of copper right bipyramids using planar twinned seeds, a high yield of right bipyramids with many parallel twins (more than 1) is obtained.[55] These observations suggest that there is scope to control the number of parallel twin boundaries (even or odd), and hence the final shape, more precisely. Furthermore, it suggests that the yield of twinned nanocubes might be further optimized by tuning the growth kinetics.

Impact of Twin Boundaries on the Facets of Nanocubes. In addition to controlling the shape symmetry, as shown in Figure 9, we observe that twinning defects also affect the facet growth, which in the case of twinned cubes are {100} side facets and potential {111} corner facets. To quantify the influence of twin planes on facet growth and shape symmetry, we define two parameters here, $R_{\{100\}}$ and $R_{\{111\}}$.

$R_{\{100\}}$ denotes the ratio of {100} facet length to width in the ⟨100⟩ zone axis, which is effectively the aspect ratio of the nanocube (Figure 10B).

$R_{\{111\}}$ denotes the ratio of {111} facet dimensions, in particular the length of {111} facets intersecting with twin planes to the length of {111} facets parallel to the twin planes as measured in the ⟨110⟩ direction (Figure 10C).

As summarized in Figure 10A, the ratio $R_{\{100\}}$ is very close to 1 (1.0 ± 0.0), suggesting that growth rates along different ⟨001⟩ directions are equivalent. However, the ratio $R_{\{111\}}$ is significantly larger than 1 (1.9 ± 0.4). The longer {111} facets intersect with twin planes, indicating a faster deposition on the {111} facets that are parallel to the twin planes.

Furthermore, we consider the impact of twin boundaries on the morphology and facets of nanocubes grown from the "reported "single-crystal" gold nanocube synthesis," which we characterized above to be a mix of single-crystal nanocubes and twinned nanocubes (Figure 8). The single-crystal nanocubes and twinned nanocubes are both grown from the reported synthesis and so have identical chemical and kinetic environments, providing an ideal system to investigate the impact of twin planes on nanocube morphology and shape (Figure 11). Within the reported synthesis, there is no significant difference in the size distribution between single-crystal cubes and twinned cubes. All of the cubes, either single crystal or twinned, are measured to have an aspect ratio (length/width) very close to 1, suggesting that equivalent growth rates prevail in each of the six ⟨100⟩ directions.

Within the same reported synthesis, there is a significant difference between the shape of the corners of single-crystal and twinned nanocubes. The growth from single-crystal cuboctahedral seeds into cubes requires a faster deposition of atoms on {111} facets than {100} facets. The single-crystal cube has relatively sharp corners (Figure 11A) (although not perfectly sharp because atoms at vertices will have higher energy[56]). In contrast, twinned cubes have truncated corners, with {111} truncation facets (Figure 11C,D). Due to the formation of lamellar twins, the nanoparticle symmetry is broken, and growth rates in ⟨111⟩ directions perpendicular to the twin lamella become slightly faster than in other previously symmetry equivalent ⟨111⟩ directions (Figure 11f), consistent with the observations in the post-seed synthesis. These {111} truncations might be caused by the "groove" ("groove" refers to the concave or convex faces created due to the mini re-entrant {111} facets formed at the particle surface near twin planes) at the edge of the twin lamella (Figure S9) so that {111} facets do not appear at corners parallel to the twin lamella. Surface grooves have been shown to play an important role in the growth kinetics of nanoplates.[21,32,33] In addition to shape control, the atoms at the "groove" tip have been shown to exhibit higher oxygen binding energies, acting as active sites for preferential oxidation.[36]

The mix of single-crystal gold nanocubes and twinned gold nanocubes with similar sizes from the reported synthesis might be used as a system to study the role of twinning defects in the mechanical or optical properties or reactivity of nanoparticles.[57−59] However, shape differences in {111} facets resulting from twin boundaries should be carefully considered.

We also investigated whether there is any correlation between the thickness of the twin lamellae and the shape of the cubes. We compared twinned cubes (we choose the post-seed crystal control synthesis as it gives a much higher percentage of twinned nanocubes) for which the twin lamella thickness varies from 4 atomic layers to 15 atomic layers (Figure S10) but did not observe any evidence of a correlation between the twin lamella width and the size, aspect ratio and degree of corner truncations of twinned cubes.

The presence of twinning defects might introduce internal strain in nanocrystals,[32] which might explain their enhanced catalytic activities. This can be seen from Figures 5B,D and 6F, where the atomic structure of most segments can be unambiguously resolved, suggesting an exact zone-axis orientation of these particles. Therefore, the loss of explicit two-dimensional atomic resolution of some segments can be attributed to the slight misorientation of these segments relative to the electron beam due to the internal strain.

Twin Detection—How Could They Be Missed? It is particularly surprising that twin boundaries are found to be prevalent in the reported syntheses of nominally single-crystal nanocubes of fcc metals. In our analysis here, ∼20% of cubes in the reported seed-mediated synthesis of nominally single-crystal gold nanocubes were found to contain twins. While reviewing TEM images in the literature, we observed that some nanocubes, which were assumed to be single crystals, in fact also exhibit similar stripe contrast suggesting that they also contain lamellar twin planes. With careful inspection, this is found to be visible in the TEM images of gold nanocubes,[23,40] copper nanocubes,[55,60] silver nanocubes,[61−63] and core−shell nanocubes.[47,64,65]

It is curious that this contrast, and hence {111} twin boundaries generating it, has not been reported previously, despite it being evident in many TEM images in the literature. In some cases, this is due to the orientation of nanocubes in which they are imaged, such as some nanocubes in Figure 1. In other cases, it may be due to the relatively weak contrast arising from twin boundaries. Also, the twin orientation is such that diffraction patterns taken from nanocubes oriented in the ⟨100⟩ zone axis will appear to be single crystals, even in the presence of twins, and this can be misleading, as shown in Figure 2B. (The ⟨100⟩ zone-axis nanocube orientation is common in TEM specimens, due to the natural orientation of the cubic shape on the support film.) Therefore, it is likely that twinning occurs more frequently in the reported syntheses of fcc metal nanocubes than has previously been reported. The

https://doi.org/10.1021/acs.chemmater.1c02459
Chem. Mater. 2021, 33, 9152−9164

simplest method for checking the presence of twinning in nanocubes is to take diffraction patterns in zone axes other than the ⟨100⟩; to use phase-contrast imaging modes, such as BF-STEM or TEM with objective apertures to maximize contrast; and by tilting nanocubes away from the ⟨100⟩ zone axis to examine changes in image contrast.

CONCLUSIONS

In summary, we introduce post-seed incorporation of twin planes, opening new routes for controlling nanocrystal morphology. Starting with single-crystal seeds, we incorporate lamellar twin planes in the growth environment with CTAB, resulting in twinned nanocubes and right bipyramids. The resolution of a broad variety of multiple twin configurations into highly specific twin geometries and associated particle shapes is significant and suggests that these are energetically favorable geometries. In this way the crystallinity of the final products can be chosen to be different to the crystallinity of the initial seeds. This post-seed incorporation of twin planes controls nanoparticle symmetry, while the nucleation and growth environments control facet growth. Together, these determine the final morphology. This approach allows control of crystallinity during both pre- and post-seed growth. This increases the possible permutations of crystallinity and facet-directing surfactants, so that new nanocrystal morphologies may be possible. Furthermore, we found that the insertion of twin planes leads to the formation of asymmetric {111} facets at cube corners; however, they have no detectable impact on the growth of {100} facets.

Finally, we found that gold nanocubes grown from syntheses that were previously reported to be single crystal, in fact, comprise a significant percentage of twinned nanocubes. We note that TEM images in the literature of nominally single-crystal gold, silver, and copper nanocubes show the similar striped contrast along the diagonal, suggestive of the presence of twin planes. We describe how the presence of twin planes can be easily missed in TEM images and diffraction patterns of nanocubes and describe the steps required to ensure detection in TEM experiments. Given the impact of twins on nanoparticle morphology and facet structure, this can be significant for their potential plasmonic and catalytic properties.

EXPERIMENTAL DETAILS

Gold(III) chloride trihydrate ($HAuCl_4 \cdot 3H_2O$) (≥99.9%), sodium borohydride ($NaBH_4$) (≥99.9%), and l-ascorbic acid (AA) (≥99.9%) were purchased from Sigma-Aldrich. Hexadecyltrimethylammonium bromide (CTAB) (98%) and ethanol (absolute, 99.5%) were purchased from Ajax Finechem. Ultrapure water (milli-Q) was used for the preparation of all solutions. Glassware was cleaned thoroughly with aqua regia prior to use.

Postseed Synthesis of Gold Nanoparticles. *Seeds.* The aqueous solutions of CTAB (1.875 mL, 0.20 M) and $HAuCl_4$ (0.025 mL, 0.050 M) were mixed with water (2.83 mL). An aqueous solution of $NaBH_4$ (0.30 mL, 0.010 M) was then rapidly added into the gold solution with vigorous stirring for 10 min. The resulting seed solution was kept at 28 ± 1 °C for 40 min prior to use.

Growth. The aqueous solutions of CTAB (1.0 mL, 0.20 M) and $HAuCl_4$ (0.10 mL, 0.050 M) were mixed with water (11.38 mL). The resultant solution was thoroughly stirred and allowed to sit for 5 min for homogenization. An aqueous solution of ascorbic acid (1.50 mL, 0.10 M) was then added, and the solution was mixed thoroughly and allowed to sit for a further 5 min. Finally, the seed solution (0.025 mL) was diluted 10 times and then immediately added with thorough mixing. The final solution was grown at 28 ± 1 °C for 48 h.

Reported Synthesis of Gold Nanocubes. Single-crystal gold nanocubes were synthesized according to reported literature methods.[12,40]

Seeds. The aqueous solutions of CTAB (1.875 mL, 0.20 M) and $HAuCl_4$ (0.025 mL, 0.050 M) were mixed with water (2.83 mL). An aqueous solution of $NaBH_4$ (0.30 mL, 0.010 M) was then rapidly added into the gold solution with vigorous stirring for 10 min. The resulting seed solution was kept at 28 ± 1 °C for 40 min prior to use.

Growth. The aqueous solutions of CTAB (3.20 mL, 0.10 M) and $HAuCl_4$ (0.080 mL, 0.05 M) were mixed with water (16.0 mL). The solution was thoroughly stirred and allowed to sit for 5 min for homogenization. An aqueous solution of ascorbic acid (1.90 mL, 0.10 M) was then added, and the solution was mixed thoroughly and allowed to sit for a further 5 min. Finally, the seed solution (0.001 mL) was diluted 100 times and then immediately added with thorough mixing. The final solution was grown at 28 ± 1 °C for 48 h.

Preparation of TEM Specimens. Ultrathin carbon (or graphene)-coated Cu TEM grids were plasma-cleaned in H_2/O_2 for 30 s before use. A sample of the growth solution was taken and immediately dropped onto the TEM grid and allowed to sit for 5 min (or for 15 s in the case of preparation of nanoparticles samples at the early stages of growth), followed by a wash in an ethanol bath and dried. Fully grown solutions (48 h) were centrifuged and redispersed in water before deposition, while products removed at earlier times in the synthesis were directly deposited on grids. The sample deposited grids were washed in a bath of ethanol (spectroscopy grade) for 20 min to remove excess CTAB.

Transmission Electron Microscopy. Electron microscopy was carried out at the Monash Centre for Electron Microscopy (MCEM) using an FEI Tecnai G2 F20 S-Twin FEG-TEM @ 200 kV for yield and shape measurements and on a FEI Titan3 80-300 FEG-TEM equipped with probe and imaging spherical aberration correctors for (S)TEM imaging at an atomic scale. All images and diffraction patterns were taken at 300 kV and STEM images used a 15 mrad probe-forming aperture. During the acquisition of the multimode tomography data set, a tilt series of projection images were acquired using two different ADF detectors, over a tilt range of −72 to +76° with a tilt increment of 2°. The tilt series were reconstructed using the ASTRA toolbox implementation of the Expectation−Maximization algorithm.[66,67] The HAADF-STEM reconstruction is used to retrieve the morphology of the nanocube, and the LAADF-STEM tilt series contains the defect information, which allows visualization of the twin lamella.

ASSOCIATED CONTENT

Supporting Information

The Supporting Information is available free of charge at https://pubs.acs.org/doi/10.1021/acs.chemmater.1c02459.

Movie of tomography tilt series (MPG)

Example HAADF-STEM and LAADF-STEM images in the tomography tilt series; images of right bipyramids containing twin lamellae; images of penta-twinned rods; and twinned nanocubes with different lamella thickness (PDF)

AUTHOR INFORMATION

Corresponding Authors

Weilun Li − *Department of Materials Science and Engineering, Monash University, Melbourne, Victoria 3800, Australia*; Email: weilun.li@monash.edu

Alison M. Funston − *School of Chemistry and ARC Centre of Excellence in Exciton Science, Monash University, Melbourne, Victoria 3800, Australia*; orcid.org/0000-0002-4320-6434; Email: alison.funston@monash.edu

Joanne Etheridge − *Department of Materials Science and Engineering, Monash University, Melbourne, Victoria 3800,*

Australia; Monash Centre for Electron Microscopy, Monash University, Melbourne, Victoria 3800, Australia; orcid.org/0000-0002-3199-3936; Email: joanne.etheridge@monash.edu

Authors

Wenming Tong − *School of Chemistry, Monash University, Melbourne, Victoria 3800, Australia;* Present Address: School of Chemistry and Energy Research Centre, Ryan Institute, National University of Ireland Galway, H91 TK33 Galway, Ireland; orcid.org/0000-0002-4831-4960

Anchal Yadav − *School of Chemistry and ARC Centre of Excellence in Exciton Science, Monash University, Melbourne, Victoria 3800, Australia;* orcid.org/0000-0003-1307-5899

Eva Bladt − *Electron Microscopy for Materials Science (EMAT) and NANOlab Center of Excellence, University of Antwerp, 2020 Antwerp, Belgium;* Present Address: DENSsolutions, Informaticalaan 12, Delft 2628 ZD, South Holland, The Netherlands.

Sara Bals − *Electron Microscopy for Materials Science (EMAT) and NANOlab Center of Excellence, University of Antwerp, 2020 Antwerp, Belgium;* orcid.org/0000-0002-4249-8017

Complete contact information is available at: https://pubs.acs.org/10.1021/acs.chemmater.1c02459

Notes

The authors declare no competing financial interest.

■ ACKNOWLEDGMENTS

This work was supported by the Australian Research Council (ARC) Grants DP160104679 and CE170100026 and used microscopes at the Monash Centre for Electron Microscopy funded by ARC Grants LE0454166, LE110100223, and LE140100104. W.L. thanks the support of the Australian Government Research Training Program (RTP) scholarship. W.T. thanks the Australian Department of Education and Monash University for the IPRS and APA scholarships. E.B. acknowledges financial support and a post-doctoral grant from the Research Foundation Flanders (FWO, Belgium). The authors thank Dr. Matthew Weyland and Dr. Tim Peterson for helpful discussions. A.Y. thanks the support from Post Graduation Publication Award (PPA) scholarship from Monash University.

■ REFERENCES

(1) Zijlstra, P.; Chon, J. W. M.; Gu, M. Five-Dimensional Optical Recording Mediated by Surface Plasmons in Gold Nanorods. *Nature* **2009**, *459*, 410−413.
(2) Barrow, S. J.; Funston, A. M.; Wei, X.; Mulvaney, P. DNA-Directed Self-Assembly and Optical Properties of Discrete 1D, 2D and 3D Plasmonic Structures. *Nano Today* **2013**, *8*, 138−167.
(3) Kauranen, M.; Zayats, A. V. Nonlinear Plasmonics. *Nat. Photonics* **2012**, *6*, 737−748.
(4) Anker, J. N.; et al. Biosensing with Plasmonic Nanosensors. *Nat. Mater.* **2008**, *7*, 442−453.
(5) Saha, K.; Agasti, S. S.; Kim, C.; Li, X.; Rotello, V. M. Gold Nanoparticles in Chemical and Biological Sensing. *Chem. Rev.* **2012**, *112*, 2739−2779.
(6) Hutchings, G. J.; Brust, M.; Schmidbaur, H. Gold-an Introductory Perspective. *Chem. Soc. Rev.* **2008**, *37*, 1759−1765.
(7) Sardar, R.; Funston, A. M.; Mulvaney, P.; Murray, R. W. Gold Nanoparticles: Past, Present, and Future. *Langmuir* **2009**, *25*, 13840−13851.
(8) Wu, B.; Zheng, N. Surface and Interface Control of Noble Metal Nanocrystals for Catalytic and Electrocatalytic Applications. *Nano Today* **2013**, *8*, 168−197.
(9) Cheng, Y.; Samia, A. C.; Meyers, J. D.; Panagopoulos, I.; Fei, B.; Burda, C. Highly Efficient Drug Delivery with Gold Nanoparticle Vectors for in Vivo Photodynamic Therapy of Cancer. *J. Am. Chem. Soc.* **2008**, *130*, 10643−10647.
(10) Jain, P. K.; Huang, X.; El-Sayed, I. H.; El-Sayed, M. A. Noble Metals on the Nanoscale: Optical and Photothermal Properties and Some Applications in Imaging, Sensing, Biology, and Medicine. *Acc. Chem. Res.* **2008**, *41*, 1578−1586.
(11) Dreaden, E. C.; Alkilany, A. M.; Huang, X.; Murphy, C. J.; El-Sayed, M. A. The Golden Age: Gold Nanoparticles for Biomedicine. *Chem. Soc. Rev.* **2012**, *41*, 2740−2779.
(12) Sau, T. K.; Murphy, C. J. Room Temperature, High-Yield Synthesis of Multiple Shapes of Gold Nanoparticles in Aqueous Solution. *J. Am. Chem. Soc.* **2004**, *126*, 8648−8649.
(13) Zhang, Q.; Xie, J.; Yu, Y.; Yang, J.; Lee, J. Y. Tuning the Crystallinity of Au Nanoparticles. *Small* **2010**, *6*, 523−527.
(14) Wang, Y.; Peng, H. C.; Liu, J.; Huang, C. Z.; Xia, Y. Use of Reduction Rate as a Quantitative Knob for Controlling the Twin Structure and Shape of Palladium Nanocrystals. *Nano Lett.* **2015**, *15*, 1445−1450.
(15) Barnard, A. S. Direct Comparison of Kinetic and Thermodynamic Influences on Gold Nanomorphology. *Acc. Chem. Res.* **2012**, *45*, 1688−1697.
(16) Xia, Y.; Xiong, Y.; Lim, B.; Skrabalak, S. E. Shape-Controlled Synthesis of Metal Nanocrystals: Simple Chemistry Meets Complex Physics? *Angew. Chem., Int. Ed.* **2009**, *48*, 60−103.
(17) Personick, M. L.; Mirkin, C. A. Making Sense of the Mayhem behind Shape Control in the Synthesis of Gold Nanoparticles. *J. Am. Chem. Soc.* **2013**, *135*, 18238−18247.
(18) Wiley, B.; Sun, Y.; Xia, Y. Synthesis of Silver Nanostructures with Controlled Shapes and Properties. *Acc. Chem. Res.* **2007**, *40*, 1067−1076.
(19) Xiong, Y.; Cai, H.; Yin, Y.; Xia, Y. Synthesis and Characterization of Fivefold Twinned Nanorods and Right Bipyramids of Palladium. *Chem. Phys. Lett.* **2007**, *440*, 273−278.
(20) Liu, M.; Guyot-Sionnest, P. Mechanism of Silver(I)-Assisted Growth of Gold Nanorods and Bipyramids. *J. Phys. Chem. B* **2005**, *109*, 22192−22200.
(21) Marks, L. D.; Peng, L. Nanoparticle Shape, Thermodynamics and Kinetics. *J. Phys.: Condens. Matter* **2016**, *28*, No. 053001.
(22) Sun, Y.; Xia, Y. Shape-Controlled Synthesis of Gold and Silver Nanoparticles. *Science* **2002**, *298*, 2176−2179.
(23) Dovgolevsky, E.; Haick, H. Direct Observation of the Transition Point between Quasi-Spherical and Cubic Nanoparticles in a Two-Step Seed-Mediated Growth Method. *Small* **2008**, *4*, 2059−2066.
(24) Zhang, J.; Langille, M. R.; Personick, M. L.; Zhang, K.; Li, S.; Mirkin, C. A. Concave Cubic Gold Nanocrystals with High-Index Facets. *J. Am. Chem. Soc.* **2010**, *132*, 14012−14014.
(25) Xia, X.; Xia, Y. Symmetry Breaking during Seeded Growth of Nanocrystals. *Nano Lett.* **2012**, *12*, 6038−6042.
(26) Gilroy, K. D.; Peng, H. C.; Yang, X.; Ruditskiy, A.; Xia, Y. Symmetry Breaking during Nanocrystal Growth. *Chem. Commun.* **2017**, *53*, 4530−4541.
(27) Lin, Q. Y.; Li, Z.; Brown, K. A.; O'Brien, M. N.; Ross, M. B.; Zhou, Y.; Butun, S.; Chen, P. C.; Schatz, G. C.; Dravid, V. P.; Aydin, K.; Mirkin, C. A. Strong Coupling between Plasmonic Gap Modes and Photonic Lattice Modes in DNA-Assembled Gold Nanocube Arrays. *Nano Lett.* **2015**, *15*, 4699−4703.
(28) Park, J. E.; Lee, Y.; Nam, J. M. Precisely Shaped, Uniformly Formed Gold Nanocubes with Ultrahigh Reproducibility in Single-Particle Scattering and Surface-Enhanced Raman Scattering. *Nano Lett.* **2018**, *18*, 6475−6482.

(29) Matteini, P.; De Angelis, M.; Ulivi, L.; Centi, S.; Pini, R. Concave Gold Nanocube Assemblies as Nanotraps for Surface-Enhanced Raman Scattering-Based Detection of Proteins. *Nanoscale* **2015**, *7*, 3474−3480.
(30) Walsh, M. J.; Barrow, S. J.; Tong, W.; Funston, A. M.; Etheridge, J. Symmetry Breaking and Silver in Gold Nanorod Growth. *ACS Nano* **2015**, *9*, 715−724.
(31) Wiley, B. J.; Xiong, Y.; Li, Z. Y.; Yin, Y.; Xia, Y. Right Bipyramids of Silver: A New Shape Derived from Single Twinned Seeds. *Nano Lett.* **2006**, *6*, 765−768.
(32) Elechiguerra, J. L.; Reyes-Gasga, J.; Yacaman, M. J. The Role of Twinning in Shape Evolution of Anisotropic Noble Metal Nanostructures. *J. Mater. Chem.* **2006**, *16*, 3906−3919.
(33) Tan, T.; Zhang, S.; Wang, J.; Zheng, Y.; Lai, H.; Liu, J.; Qin, F.; Wang, C. Resolving the Stacking Fault Structure of Silver Nanoplates. *Nanoscale* **2021**, *13*, 195−205.
(34) Personick, M. L.; Langille, M. R.; Zhang, J.; Wu, J.; Li, S.; Mirkin, C. A. Plasmon-Mediated Synthesis of Silver Cubes with Unusual Twinning Structures Using Short Wavelength Excitation. *Small* **2013**, *9*, 1947−1953.
(35) Wang, C. W.; Sun, X.; Chang, H. T.; Qin, D. Generation of Enzymatic Hydrogen Peroxide to Accelerate the Etching of Silver Nanocrystals with Selectivity. *Chem. Mater.* **2016**, *28*, 7519−7527.
(36) Zhu, Q.; Pan, Z.; Zhao, Z.; Cao, G.; Luo, L.; Ni, C.; Wei, H.; Zhang, Z.; Sansoz, F.; Wang, J. Defect-Driven Selective Metal Oxidation at Atomic Scale. *Nat. Commun.* **2021**, *12*, No. 558.
(37) Xia, X.; Choi, S.; Herron, J. A.; Lu, N.; Scaranto, J.; Peng, H. C.; Wang, J.; Mavrikakis, M.; Kim, M. J.; Xia, Y. Facile Synthesis of Palladium Right Bipyramids and Their Use as Seeds for Overgrowth and as Catalysts for Formic Acid Oxidation. *J. Am. Chem. Soc.* **2013**, *135*, 15706−15709.
(38) Zhou, W.; Wu, J.; Yang, H. Highly Uniform Platinum Icosahedra Made by Hot Injection-Assisted GRAILS Method. *Nano Lett.* **2013**, *13*, 2870−2874.
(39) Zhu, D.; Yan, J.; Xie, J.; Liang, Z.; Bai, H. Ultrafast Laser-Induced Atomic Structure Transformation of Au Nanoparticles with Improved Surface Activity. *ACS Nano* **2021**, *15*, 13140−13147.
(40) Wu, X.; Ming, T.; Wang, X.; Wang, P.; Wang, J.; Chen, J. High-Photoluminescence-Yield Gold Nanocubes: For Cell Imaging and Photothermal Therapy. *ACS Nano* **2010**, *4*, 113−120.
(41) Katz-Boon, H.; Rossouw, C. J.; Dwyer, C.; Etheridge, J. Rapid Measurement of Nanoparticle Thickness Profiles. *Ultramicroscopy* **2013**, *124*, 61−70.
(42) Winckelmans, N.; Altantzis, T.; Grzelczak, M.; Sánchez-Iglesias, A.; Liz-Marzán, L. M.; Bals, S. Multimode Electron Tomography as a Tool to Characterize the Internal Structure and Morphology of Gold Nanoparticles. *J. Phys. Chem. C* **2018**, *122*, 13522−13528.
(43) Marks, L. D. Modified Wulff Constructions for Twinned Particles. *J. Cryst. Growth* **1983**, *61*, 556−566.
(44) Gontard, L. C.; Dunin-Borkowski, R. E.; Gass, M. H.; Bleloch, A. L.; Ozkaya, D. Three-Dimensional Shapes and Structures of Lamellar-Twinned Fcc Nanoparticles Using ADF STEM. *J. Electron Microsc.* **2009**, *58*, 167−174.
(45) McEachran, M.; Kitaev, V. Direct Structural Transformation of Silver Platelets into Right Bipyramids and Twinned Cube Nanoparticles: Morphology Governed by Defects. *Chem. Commun.* **2008**, *44*, 5737−5739.
(46) Zhang, J.; Liu, J.; Xie, Z. X.; Qin, D. HAuCl4: A Dual Agent for Studying the Chloride-Assisted Vertical Growth of Citrate-Free Ag Nanoplates with Au Serving as a Marker. *Langmuir* **2014**, *30*, 15520−15530.
(47) Shi, Y.; Lyu, Z.; Liu, J.; Chase, E.; Xia, Y. Facile Synthesis of Pd−Cu Bimetallic Twin Nanocubes and a Mechanistic Understanding of the Shape Evolution. *ChemNanoMat* **2020**, *6*, 386−391.
(48) Johnson, C. J.; Dujardin, E.; Davis, S. A.; Murphy, C. J.; Mann, S. Growth and Form of Gold Nanorods Prepared by Seed-Mediated, Surfactant-Directed Synthesis. *J. Mater. Chem.* **2002**, *12*, 1765−1770.
(49) Huo, D.; Kim, M. J.; Lyu, Z.; Shi, Y.; Wiley, B. J.; Xia, Y. One-Dimensional Metal Nanostructures: From Colloidal Syntheses to Applications. *Chem. Rev.* **2019**, *119*, 8972−9073.
(50) Huo, D.; Cao, Z.; Li, J.; Xie, M.; Tao, J.; Xia, Y. Seed-Mediated Growth of Au Nanospheres into Hexagonal Stars and the Emergence of a Hexagonal Close-Packed Phase. *Nano Lett.* **2019**, *19*, 3115−3121.
(51) Lu, S.; Liang, J.; Long, H.; Li, H.; Zhou, X.; He, Z.; Chen, Y.; Sun, H.; Fan, Z.; Zhang, H. Crystal Phase Control of Gold Nanomaterials by Wet-Chemical Synthesis. *Acc. Chem. Res.* **2020**, *53*, 2106−2118.
(52) Zhang, G.; Jasinski, J. B.; Howell, J. L.; Patel, D.; Stephens, D. P.; Gobin, A. M. Tunability and Stability of Gold Nanoparticles Obtained from Chloroauric Acid and Sodium Thiosulfate Reaction. *Nanoscale Res. Lett.* **2012**, *7*, No. 337.
(53) Grzelczak, M.; Pérez-Juste, J.; Mulvaney, P.; Liz-Marzán, L. M. Shape Control in Gold Nanoparticle Synthesis. *Chem. Soc. Rev.* **2008**, *37*, 1783−1791.
(54) Zhang, L.; Zhao, Y.; Lin, Z.; Gu, F.; Lau, S. P.; Li, L.; Chai, Y. Kinetically Controlled Synthesis of Large-Scale Morphology-Tailored Silver Nanostructures at Low Temperature. *Nanoscale* **2015**, *7*, 13420−13426.
(55) Lyu, Z.; Xie, M.; Gilroy, K. D.; Hood, Z. D.; Zhao, M.; Zhou, S.; Liu, J.; Xia, Y. A Rationally Designed Route to the One-Pot Synthesis of Right Bipyramidal Nanocrystals of Copper. *Chem. Mater.* **2018**, *30*, 6469−6477.
(56) Sneed, B. T.; Young, A. P.; Tsung, C. K. Building up Strain in Colloidal Metal Nanoparticle Catalysts. *Nanoscale* **2015**, *7*, 12248−12265.
(57) Tang, Y.; Ouyang, M. Tailoring Properties and Functionalities of Metal Nanoparticles through Crystallinity Engineering. *Nat. Mater.* **2007**, *6*, 754−759.
(58) Aherne, D.; Ledwith, D. M.; Gara, M.; Kelly, J. M. Optical Properties and Growth Aspects of Silver Nanoprisms Produced by a Highly Reproducible and Rapid Synthesis at Room Temperature. *Adv. Funct. Mater.* **2008**, *18*, 2005−2016.
(59) Yang, Z.; Zhang, G.; Luo, G.; Sun, X.; Zhao, J. Mechanical Properties of Gold Twinned Nanocubes under Different Triaxial Tensile Rates. *Phys. Lett. A* **2016**, *380*, 2674−2677.
(60) Lisiecki, I. Size, Shape, and Structural Control of Metallic Nanocrystals. *J. Phys. Chem. B* **2005**, *109*, 12231−12244.
(61) Zhang, W. C.; Wu, X. L.; Chen, H. T.; Gao, Y. J.; Zhu, J.; Huang, G. S.; Chu, P. K. Self-Organized Formation of Silver Nanowires, Nanocubes and Bipyramids via a Solvothermal Method. *Acta Mater.* **2008**, *56*, 2508−2513.
(62) Park, H. G.; Joo, J. H.; Kim, H. G.; Lee, J. S. Shape-Dependent Reversible Assembly Properties of Polyvalent DNA-Silver Nanocube Conjugates. *J. Phys. Chem. C* **2012**, *116*, 2278−2284.
(63) Polavarapu, L.; Liz-Marzán, L. M. Growth and Galvanic Replacement of Silver Nanocubes in Organic Media. *Nanoscale* **2013**, *5*, 4355−4361.
(64) Guo, H.; Chen, Y.; Ping, H.; Jin, J.; Peng, D. L. Facile Synthesis of Cu and Cu@Cu-Ni Nanocubes and Nanowires in Hydrophobic Solution in the Presence of Nickel and Chloride Ions. *Nanoscale* **2013**, *5*, 2394−2402.
(65) Lyu, Z.; Xie, M.; Aldama, E.; Zhao, M.; Qiu, J.; Zhou, S.; Xia, Y. Au@Cu Core-Shell Nanocubes with Controllable Sizes in the Range of 20-30 Nm for Applications in Catalysis and Plasmonics. *ACS Appl. Nano Mater.* **2019**, *2*, 1533−1540.
(66) Moon, T. K. The Expectation Maximization Algorithm. *IEEE Signal Process. Mag.* **1996**, *13*, 47−60.
(67) van Aarle, W.; Palenstijn, W. J.; De Beenhouwer, J.; Altantzis, T.; Bals, S.; Batenburg, K. J.; Sijbers, J. The ASTRA Toolbox: A Platform for Advanced Algorithm Development in Electron Tomography. *Ultramicroscopy* **2015**, *157*, 35−47.

https://doi.org/10.1021/acs.chemmater.1c02459
Chem. Mater. 2021, 33, 9152−9164